Aerospace Science and Technology 144 (2024) 108732

Contents lists available at ScienceDirect

Aerospace Science and Technology

journal homepage: www.elsevier.com/locate/aescte

Approach and landing guidance using constrained model predictive static programming

Aysha S. Hameed [a,*], Bindu G . R . [a], Srianish Vutukuri [b]

[a] Department of Electrical Engineering, College of Engineering Trivandrum, Kerala, India
[b] Department of Aerospace Engineering, Indian Institute of Science, Bangalore, India

ARTICLE INFO

Editor: Roberto Sabatini

Keywords:
Approach and landing
Constrained model predictive static programming
Unpowered reusable launch vehicles
Guidance
Dynamic inversion

ABSTRACT

The paper proposes a guidance scheme during the approach and landing phase of an unpowered vehicle to achieve high precision at touchdown by limiting the control inputs within allowable bounds using constrained Model Predictive Static Programming. The advantages of a single flight phase are incorporated into the design since the guess control history is obtained from a single segment based guidance approach. The requirement of ensuring continuity in states and guidance commands are hence avoided leading to minimization of control deviations using a simple cost function. Constrained input commands are used for determining control surface deflection based on dynamic inversion considering the longitudinal pitch rate dynamics. Comparison is carried out between the results obtained for constrained as well as unconstrained schemes for the nominal trajectory. Comparisons of load factor, dynamic pressure and flight path angle for three segment, two segment, single segment guidance strategies have been carried out with MPSP based guidance to evaluate the relative advantages offered by the scheme. Performance analysis of the proposed scheme is done based on numerous simulations with simultaneous variations in initial states, vehicle parameters and aerodynamic parameter variations. Simulation results indicate that the proposed scheme is suitable for landing on runways of shorter lengths due to minimal touchdown errors.

1. Introduction

Reusable Launch Vehicles (RLVs) have proven to be a cost-effective option to travel to and return from space. The major challenge in such missions is to bring the vehicle safely back to earth. This task is complex and challenging due to varying guidance requirements during descent, from atmospheric re-entry phase to landing. Autonomous safe landing on the runway is crucial especially for manned missions, hence, careful planning and design of landing guidance strategies are fundamental for completing such missions. During the final approach and landing (A & L) phase, the main objective is the judicious use of available energy to land on the designated site satisfying the terminal constraints. The constraints on velocity, flight path angle, pitch angle, as well as altitude, need to be achieved at touchdown satisfying the bounds on the control inputs under adverse conditions.

Many of the past research has focused on developing different guidance algorithms specifically for unpowered landing on the runway. Shuttle auto-land guidance makes use of a typical trajectory consisting of fixed steep and shallow reference paths but may not be suitable to accommodate large trajectory dispersions [1]. An auto-landing program has been developed relying on steep glideslope, circular flare and exponential flare to shallow glideslope satisfying the bounds on dynamic pressure [2]. Constrained trajectory propagation is used to rapidly generate feasible trajectories using simple geometric segments [3]. A two segment path consisting of equilibrium glide followed by exponential flare maneuver which relies on interpolations of stored data (necessitates offline data storage) is introduced to control ground range by adjusting glide efficiency factor [4]. The onboard trajectory planning algorithm based on a three segment scheme iterates on flight path angle at the start of the flare and makes use of dynamic pressure matching to design a feasible path connecting the current state of the vehicle to runway touchdown [5]. The three segment scheme making use of PID (Proportional-Integral-Derivative) control to generate closed loop commands is being compared with the proposed methodology in this paper. A steep glide path followed by a quadratic polynomial-based flare maneuver is used to model the entire A & L phase [6]. This algorithm based on quadratic flare maneuver with PID control implemented for closed loop guidance commands as explained in [5] is also adopted for comparison in this paper with the proposed method. Gain scheduled

* Corresponding author at: College of Engineering Trivandrum, APJ Abdul Kalam Technological University, Kerala, India.
E-mail address: ayshahameed@cet.ac.in (A.S. Hameed).

https://doi.org/10.1016/j.ast.2023.108732
Received 31 December 2021; Received in revised form 2 April 2023; Accepted 10 November 2023
Available online 17 November 2023
1270-9638/

Nomenclature

α	angle of attack, deg
β	inverse scale height, m^{-1}
γ	flight path angle, deg
ω	pitch rate, rad/s
$\overline{c}$	Mean aerodynamic chord, m
ρ	Atmospheric density, kg/m^3
θ	pitch angle, deg
α_i	reference quintic polynomial coefficients, i = 0,1,2,3,4,5
R	distance from the center of gravity to aerodynamic center
λ	costate variable
C_M	pitching moment coefficient about aerodynamic center
C_{M0}	pitching moment coefficient at zero angle of attack
$C_{M\alpha}$	change in pitching moment coefficient due to angle of attack
$C_{M\delta e}$	change in pitching moment coefficient due to elevon deflection
C_D	drag coefficient
C_L	lift coefficient
J	cost function
R_k	positive definite matrix
h	altitude above runway, m
m	vehicle mass, kg
$Mach$	Mach Number
$\dot{h}$	sink rate, m/s
k_ω	pitch rate gain
I_{yy}	Moment of Inertia about Y axis
Δt	numerical integration step
I	identity matrix
δ_e	elevon deflection angle, deg
q	dynamic pressure, N/m^2
B	Sensitivity matrix
S	vehicle reference area, m^2
t	time, s
V	velocity of the vehicle, m/s
X	downrange position along runway centerline, m
g	acceleration due to gravity
Z	state vector
Y	output vector
U	control vector
BB	matrix used for recursive computation
dU_k	update in control at the kth step
dY_N	deviation in output from the desired terminal values
A_λ	Matrix used for computation of dU_k

Subscripts

0	sea-level value
ALI	Approach and Landing Interface
i	initial value
f	final value
d	desired value
max	maximum allowable value
min	minimum allowable value
k	discretization step
N	total discretization steps
TD	Touchdown

finite horizon LQR (Linear Quadratic Regulator) based on two segment algorithm is implemented for A & L [7]. An integrated guidance and control algorithm based on LQR with full state feedback stepping through a reference trajectory consisting of three phases of flight is designed [8]. The scheme is implemented on X34 and relies on three segment scheme to guide the vehicle to touchdown. However, an underlying requirement for multiple segment-based guidance algorithms [5–8] is that continuity in guidance commands need to be ensured as the vehicle transitions from one flight phase to another. Guidance algorithms based on Sliding Mode Control [9–11] and Optimal Path Planning using finite-SDRE (State Dependent Riccati Equation) technique [12,13] is proposed. Even though promising results are obtained with such schemes, control constraints are not being considered. Second-order cone programming [14] is developed during A & L wherein constraints are considered in the design, but the simulations presented are with respect to variations in initial conditions only. A predictor-corrector guidance method relying on a two segment method based on all-coefficient adaptive control theory is presented for generating trajectories online during landing [15]. The scheme considers terminal constraints, and the guidance law modifies the lift coefficient by applying constraints on load factor and dynamic pressure. Assessment of robust stability of an autonomous lander using a methodology employing mu-Analysis and Monte Carlo simulations are implemented [16]. This technique is applied to a case study representing a descent module during the controlled landing phase on the Mars surface. Backstepping and Dynamic Inversion based controller design have been proposed for auto-landing of a UAV (Unmanned Aerial Vehicle) during the final approach, glideslope and flare which also rely on a multiple segment scheme [17–19]. A Time and Energy (T & E) based guidance for optimized 4-D trajectory combined with a control strategy for attitude and T & E corrections is proposed for descent and approach [20]. In such a scheme, guidance and control modules allow the aircraft to follow a T&E-optimal 4D trajectory with different phases and to recover from deviations in the initial energy states. A single segment guidance algorithm relying on a quintic polynomial is designed during A & L connecting the initial states of the vehicle to runway touchdown using a forward propagation algorithm [21]. The methodology presented in [21] is used to generate the guess control history in this research and is also eventually compared with the proposed method in this paper.

Non-linear optimal control theory offers an optimal solution in solving many problems, however, the complexity and dimensionality issues, poor computational efficiency and low convergence rate pose difficulty in onboard implementation. The proposed scheme in this paper addresses these issues by utilizing the inherent advantages of Model Predictive Static Programming (MPSP). MPSP combines the philosophies of Model Predictive Control and Dynamic Programming and is a computationally efficient scheme feasible for aerospace applications. MPSP helps in obtaining the solution in a faster sense by the formulation of a static costate vector and offers the viability of computation of sensitivity matrices recursively [26]. The technique is applied to various aerospace guidance applications with faster computational requirements [27–29]. Closed-loop guidance based on MPSP is proposed to increase the accuracy of satellite-carrier boosters' landing point [30]. The guidance commands for aerobatic aircraft in air race are generated using generalized model predictive static programming (G-MPSP) formulation by incorporating both state and input inequality constraints [31]. A generalized quasi-spectral model predictive static programming method is developed to improve computational efficiency wherein the spectral sensitivity matrix is then efficiently solved using the Gauss Quadrature Collocation method [32].

MPSP is also effectively used for the reentry guidance problem to bring the vehicle safely through the reentry corridor satisfying the structural, thermal as well as control constraints [22,23]. But the reentry guidance problem effectively solved using MPSP does not explore the requirement of A & L on the runway. This is because, for simpler missions, the vehicle is guided to specified final coordinates at the end of the

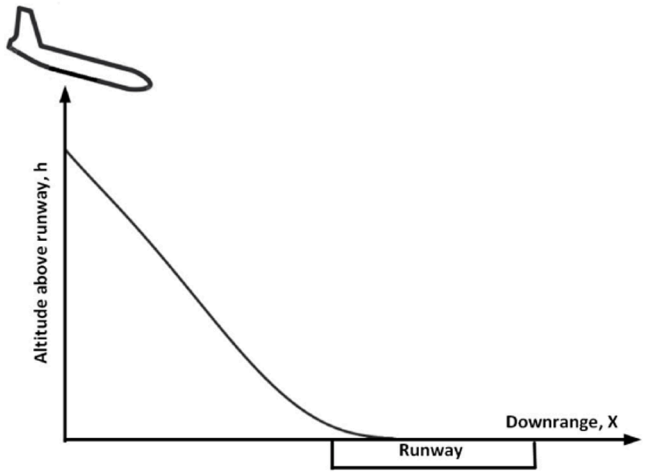

Fig. 1. Schematic representation of vehicle approaching the runway

reentry phase with reduced velocity so that it can glide to the sea with the help of a parachute [22]. However, considering manned missions, instead of landing on the sea, safe landing on the runway is preferable which is a challenging problem for an unpowered vehicle. This paper hence proposes a constrained Model Predictive Static Programming based guidance scheme for the A & L phase of the unpowered vehicle on the runway.

The contributions of the paper compared to the existing literature can be summarized as follows: (i) Instead of considering only the terminal constraints at touchdown as in many of the papers dealing with A & L trajectory design, the proposed scheme based on MPSP incorporates the constraints on input commands also in the design. Constrained control commands are crucial in such a mission so that the control surfaces are not saturated. (ii) The initial guess command history required by the MPSP algorithm is obtained based on the computationally simpler single segment guidance algorithm relying on a quintic polynomial altitude model [21]. Hence, the additional terms required in the cost function to ensure continuity and smoothness in trajectory states, as well as guidance commands, are avoided which in turn leads to minimization of a simple cost function to arrive at the solution (iii) In this paper, MPSP is being attempted for the first time for the A & L phase of an unpowered RLV on the runway. The touchdown results obtained for constrained and unconstrained MPSP are compared for the nominal trajectory. (iv) The load factor, dynamic pressure and flight path angle obtained from the proposed scheme are compared with other multiple segment and single segment schemes and the results are analyzed. The constrained MPSP scheme offers gradually varying load factor profile without steep transitions and sudden changes. The dynamic pressure for constrained MPSP is observed to be the least for major part of the downrange until touchdown. Smoothened and gradually varying flight path angle profile is obtained with constrained MPSP unlike the flight path profile obtained for multiple segment schemes. The advantages in load factor and dynamic pressure contribute to structural safety of the vehicle which is a critical concern in RLV landing. (v) Further, a comprehensive performance evaluation of precise landing on the runway during the final A & L phase is also carried out in this paper, to verify touchdown conditions under various off-nominal conditions. For simulation of off-nominal conditions, simultaneous perturbation is introduced in initial states, vehicle and aerodynamic parameters that can lead to unfavorable conditions for landing. The precision achieved in downrange with respect to the desired touchdown point under such off-nominal conditions is also highlighted. Favorable results are obtained considering the practical issues that happen on unpowered landing like tire blowout, tail scraping, colliding with runway and overrunning the runway length under off-nominal conditions.

2. Problem formulation

The vehicle considered for simulation is the X34 Technology Demonstrator with available aerodynamic data. The current scheme considers only the elevons for longitudinal control. The aerodynamic data of the vehicle is obtained using wind tunnel tests and is available in the literature [24,25]. The coefficient of lift C_L and coefficient of drag C_D can be determined by two-dimensional interpolation based on the angle of attack and Mach number from aerodynamic tables. The effect on pitching moment due to changes in elevon deflection is determined from the aerodynamic data.

The A & L phase begins at the Approach and Landing Interface (ALI) at an altitude of 10,000 feet (3048 m) above the runway. At ALI, the vehicle is aligned with the runway centerline with no cross-range errors. Under nominal conditions at ALI, the vehicle is to be guided safely to the runway at the desired touchdown point so that it does not overshoot or undershoot the runway length. However, if the vehicle arrives at ALI under off-nominal conditions, the available energy needs to be dissipated judiciously so that desired touchdown conditions are met within the specified constraints. Violation of terminal constraints can lead to undesirable effects like tail scraping, tire blowout, crashing or overshooting the runway length. Moreover, unfavorable conditions like state and aerodynamic parameter changes can lead to deviations in trajectory which need to be effectively addressed by the guidance algorithm. The evaluation of the performance of the MPSP guidance algorithm in tackling these issues is the focus of this paper.

2.1. A & L guidance problem

The unpowered vehicle is considered as a point mass. The forces acting on the vehicle are the atmospheric lift, drag as well as gravitational force. The aerodynamic center is considered aligned with the center of gravity along the X-body direction. The schematic of the vehicle approaching the runway is shown in Fig. 1. The states of the RLV during the A & L phase vary as a function of downrange X as indicated by (1)-(5) [8,13].

$$V' = \frac{dV}{dX} = -\frac{0.5\rho VSC_D}{m\cos\gamma} - \frac{g\tan\gamma}{V} \tag{1}$$

$$\gamma' = \frac{d\gamma}{dX} = \frac{0.5\rho SC_L}{m\cos\gamma} - \frac{g}{V^2} \tag{2}$$

$$\theta' = \frac{d\theta}{dX} = \frac{\omega}{V\cos\gamma} \tag{3}$$

$$\omega' = \frac{d\omega}{dX} = \frac{0.5\rho VS\overline{C_M}\bar{c}}{I_{yy}\cos\gamma} \tag{4}$$

$$h' = \frac{dh}{dX} = \tan\gamma \tag{5}$$

V is the velocity, γ is the flight path angle, θ is the pitch angle, ω is the pitch rate, h is the altitude, m is the mass of the vehicle, g is the acceleration due to gravity, ρ is the atmospheric density, $C_L$and C_D are coefficients of lift and drag respectively. The pitching moment coefficient with respect to centre of gravity, $\overline{C_M}$ in (4) is as given by (6) where α is the angle of attack and δ_e is the elevon deflection [8].

$$\overline{C_M} = C_{M0} + C_{M\alpha}\alpha + C_{M\delta_e}\,\delta_e + \frac{R(C_L\cos\alpha + C_D\sin\alpha)}{\bar{c}} \tag{6}$$

Since downrange is chosen as the independent variable, the time derivative is expressed as (7) [12].

$$t' = \frac{dt}{dX} = \frac{1}{V\cos\gamma} \tag{7}$$

Atmospheric density ρ is computed using an exponential model given

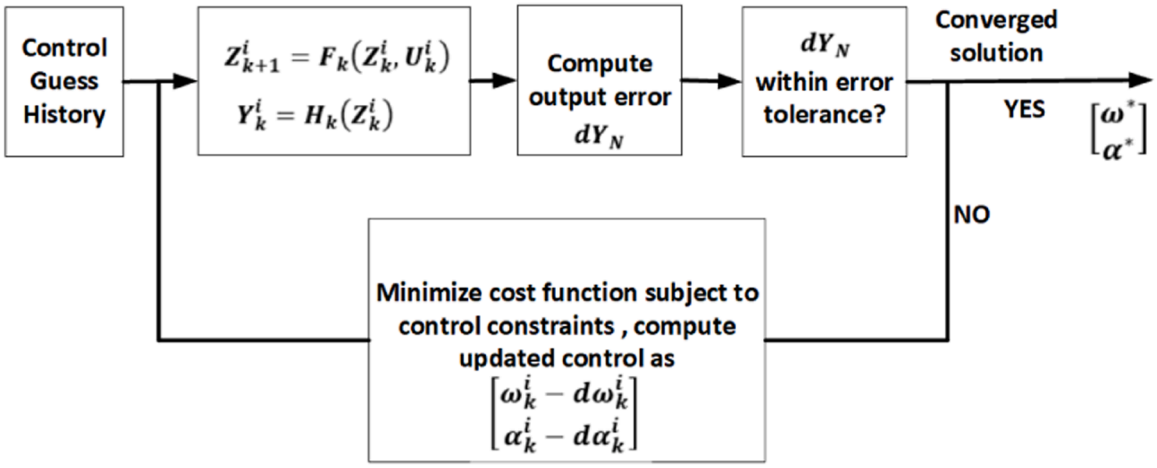

Fig. 2. Block diagram of MPSP Guidance Algorithm

Table 1
Initial states at ALI

State	Initial value
Initial velocity, V_{ALI}	190 m/s
Initial pitch angle, θ_{ALI}	-10.77 deg
Initial downrange, X_{ALI}	-19028 m
Initial altitude, h_{ALI}	3048 m

Table 2
Final desired states at touchdown

State	Final value
Touchdown velocity, V_{TD}	105 m/s
Touchdown pitch angle, θ_{TD}	5.5 deg
Touchdown downrange, X_{TD}	500 m
Touchdown altitude, h_{TD}	0 m

Table 3
Convergence criteria for output error

Velocity error	Pitch angle error	Altitude error
<1 m/s	<0.57 deg	<0.3 m

by (8) where $\rho_0$indicates the atmospheric density at sea-level and β is the inverse scale height [5].

$$\rho(h) = \rho_0 e^{-\beta h} \tag{8}$$

At touchdown, the following terminal conditions need to be satisfied where the subscript f denotes the final value and the superscript d denotes the desired values for each state.

$$V_f = V^d, \quad \theta_f = \theta^d, \quad \alpha_f = \alpha^d, \; h_f = h^d, \; X_f = X^d \tag{9}$$

The constraints at touchdown on final pitch angle and final angle of attack enforces the constraint on final flight path angle automatically since $\gamma = \theta - \alpha$. To avoid tail scrape or collision at touchdown, the angle of attack is bounded within minimum and maximum limits as given by (10). The constraint on pitch rate is as specified by (11). The limits on angle of attack is set between 0^0 and 10^0 and the pitch rate limits are set between -3 deg/sec to 3 deg/sec as per the data from reference values for the X34 [8].

$$\alpha_{min} \leq \alpha \leq \alpha_{max} \tag{10}$$

$$\omega_{min} \leq \omega \leq \omega_{max} \tag{11}$$

The longitudinal control surface (elevon) deflections are limited by minimum and maximum bounds. The pitching moment coefficient as indicated in (6) is mainly contributed by change in moment due to angle of attack α and elevon deflection δ_e and substantially influences the pitch rate dynamics expressed in (4). Hence, by limiting the angle of attack and pitch rate commands within specific bounds indicated by (10) and (11), it can be ensured that the elevon control surface does not saturate or go beyond the allowable limits. It is to be noted that the aerodynamic errors related to pitching moment dynamics are not considered here. The required elevon control surface deflection is determined using dynamic inversion from the pitch rate dynamics.

The above guidance design philosophy is inspired from the approach adopted for MPSP design during the re-entry phase, which does not explore the guidance design for A & L phase [22]. It is rational to follow the same design philosophy here since A & L is the final phase of descent and hence such an approach is judiciously adopted in this paper. But the guidance requirements for A & L are different from re-entry phase, hence the choice of control variables need to be different.

In the A & L phase, longitudinal dynamics is strongly coupled with the angle of attack, and hence angle of attack is chosen as one of the control variables. Constraints on the pitch rate need to be imposed to restrain the pitch angle in order to avoid scraping the tail or crashing. Along with angle of attack, the deflection of elevons also contribute to incremental pitching moment coefficient and hence can influence the pitch rate dynamics substantially. The limits on the elevon deflection also need to be incorporated into the design. Anyhow, constraining any two of the variables, the pitch rate and angle of attack enforces limits in the allowable elevon deflection also which is an added advantage of the guidance design. Taking these factors into consideration, the control inputs for MPSP are chosen as angle of attack and pitch rate, both of which are constrained within lower and upper bounds. The solution obtained using MPSP guidance must satisfy both the terminal constraints mentioned in (9) as well as control constraints specified by (10) and (11).

2.2. MPSP based formulation for A & L

The discretized form of system dynamics represented by (12) and (13) is considered in MPSP design. $Z_k \in \mathbb{R}^n$ represents the state vector, $U_k \in \mathbb{R}^n$ is the control vector and $Y_k \in \mathbb{R}^n$ is the output vector with $k = 1, 2 \ldots N$ being the discrete steps considered from ALI to the touchdown point. Iteration index i indicates the current iteration being carried out by the algorithm.

$$Z^i_{k+1} = F_k(Z^i_k, U^i_k) \tag{12}$$

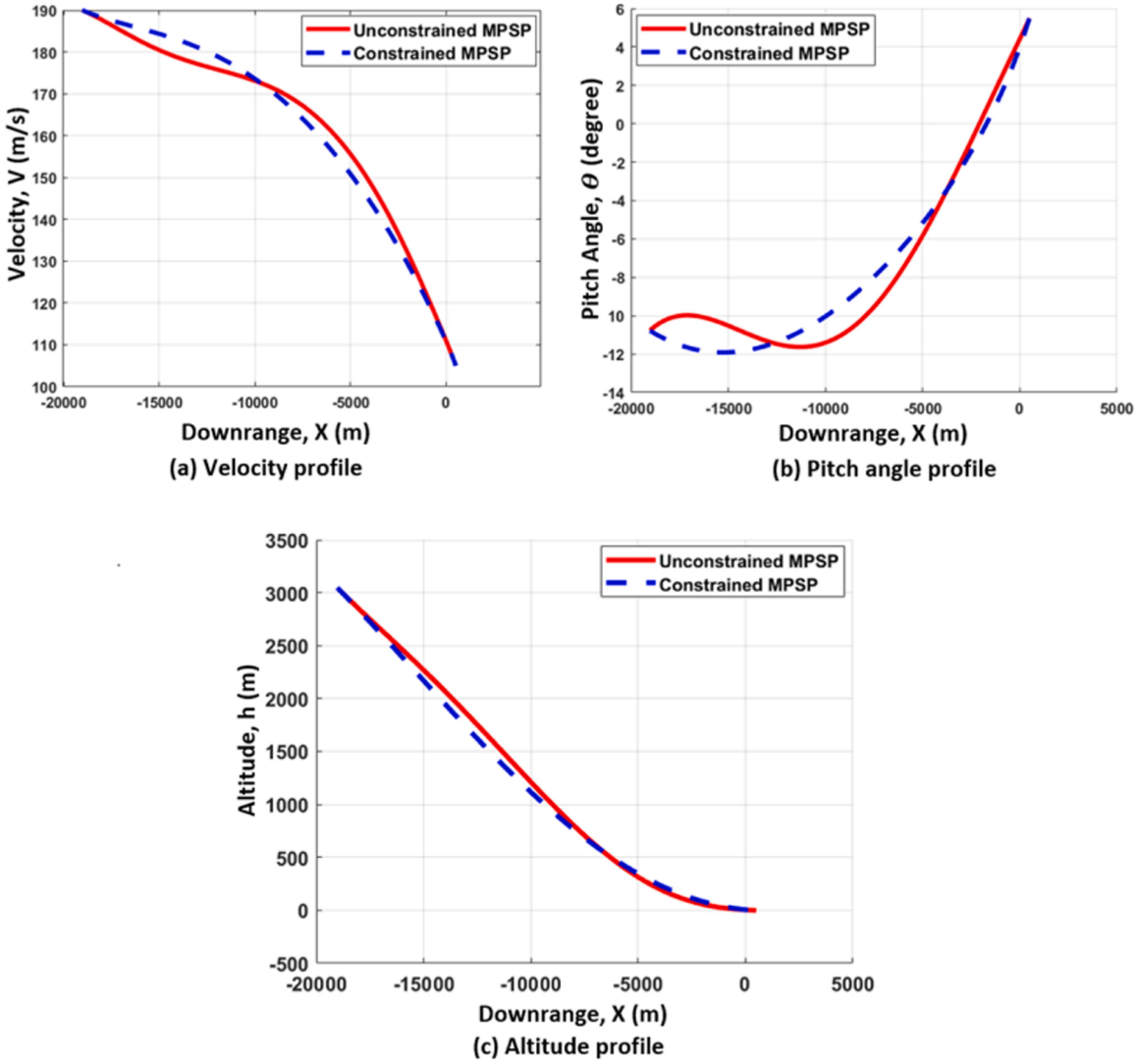

Fig. 3. Comparison of state profile for constrained and unconstrained MPSP

$$Y_k^i = H_k\left(Z_k^i\right) \tag{13}$$

The state vector, control vector and output vector for the A & L problem is selected as (14), (15) and (16) respectively.

$$Z_k^i = \begin{bmatrix} V_k^i & \theta_k^i & h_k^i \end{bmatrix}^T \tag{14}$$

$$U_k^i = \begin{bmatrix} \omega_k^i & \alpha_k^i \end{bmatrix}^T \tag{15}$$

$$Y_k^i = \begin{bmatrix} V_k^i & \theta_k^i & h_k^i \end{bmatrix}^T \tag{16}$$

The theory behind MPSP has been well explained in various previous research and is not dealt with here in detail. The block diagram explaining the iterative MPSP process is detailed in Fig. 2.

Initially, a guess control history is determined, the process is explained in detail in the next section. The control inputs are scheduled as a function of downrange along the entire A & L by considering closely spaced fixed intervals of 100 m downrange. The values at these closely spaced points serve as the initial guess control history being used by the MPSP algorithm. In order to propagate the state dynamics, the discretized state equations are written using the Euler integration approach as in (17).

$$Z_{k+1}^i = F_k\left(Z_k^i, U_k^i\right) = Z_k^i + \Delta X\, f\left(Z_k^i, U_k^i\right) \tag{17}$$

The function $f(Z_k^i, U_k^i)$ is the first order derivative function defined as (18).

$$f\left(Z_k^i, U_k^i\right) = \begin{bmatrix} V_k^{i'} & \theta_k^{i'} & h_k^{i'} \end{bmatrix} \tag{18}$$

It is to be noted that the deviation in output from the desired terminal values at the final step N for the i^{th} iteration can be written in terms of sensitivity matrices using (19) [22].

$$dY_N^i = B_1^i dU_1^i + B_2^i dU_2^i + \ldots + B_{N-1}^i dU_{N-1}^i = \sum_{k=1}^{N-1} B_k^i dU_k^i \tag{19}$$

The sensitivity matrix B_k for the i^{th} iteration (B_k^i) is given by (20). The Jacobian matrices are required for the computation of sensitivity matrices as shown in (20) [22].

$$B_k^i = \left[\frac{\partial Y_N^i}{\partial Z_N^i}\right]\left[\frac{\partial F_{N-1}^i}{\partial Z_{N-1}^i}\right]\left[\frac{\partial F_{k+1}^i}{\partial Z_{k+1}^i}\right]\left[\frac{\partial F_k^i}{\partial U_k^i}\right] \tag{20}$$

Instead of evaluating the sensitivity matrices from $k = 1, 2 \ldots . N-1$ directly, it is possible to compute them recursively for reducing the computation time [25]. The recursive computation is carried out as per the following steps indicated by (21), (22) and (23) [25].

The matrix BB_{N-1}^i is initially defined as in (21).

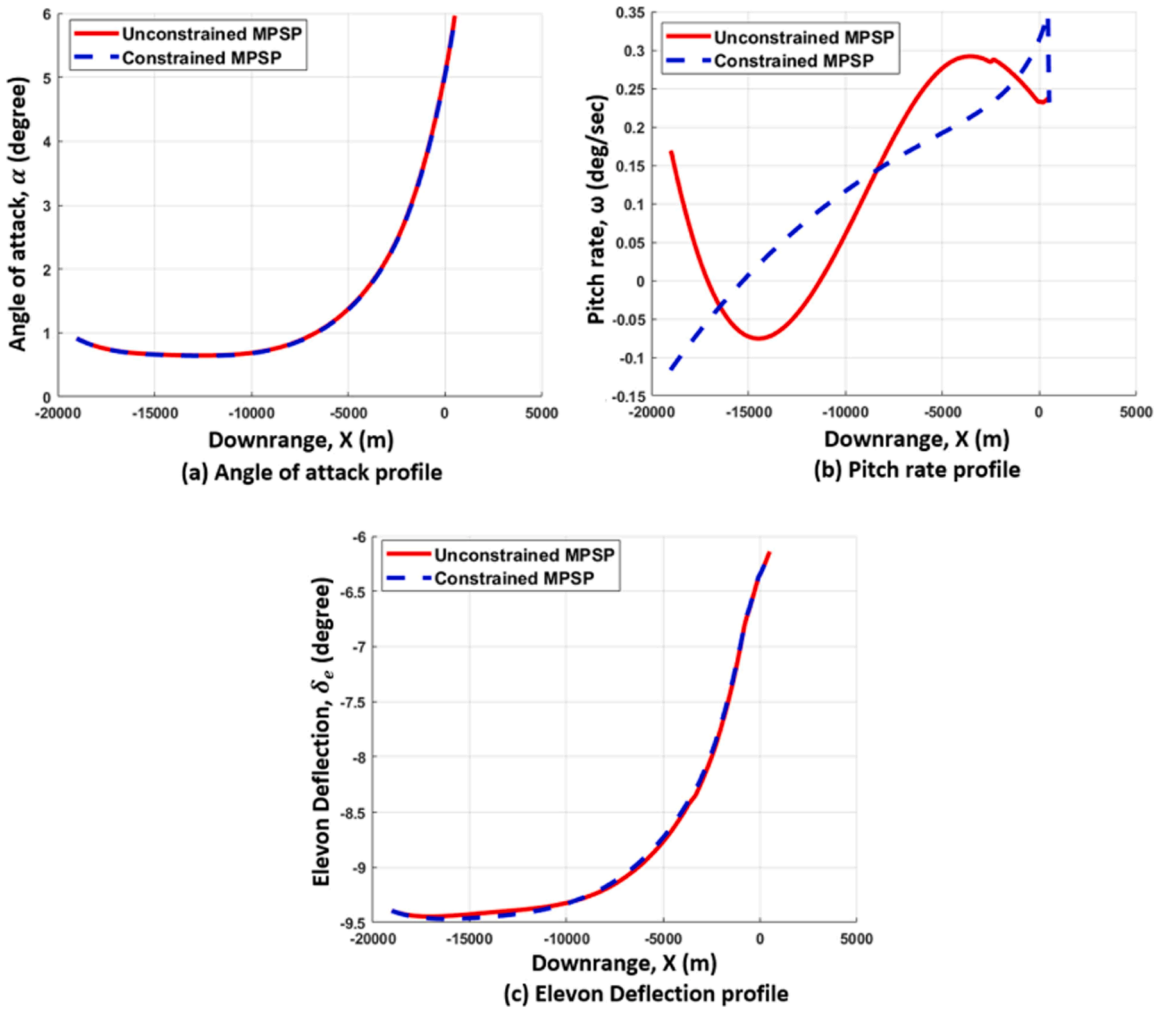

Fig. 4. Comparison of command profile for constrained and unconstrained MPSP

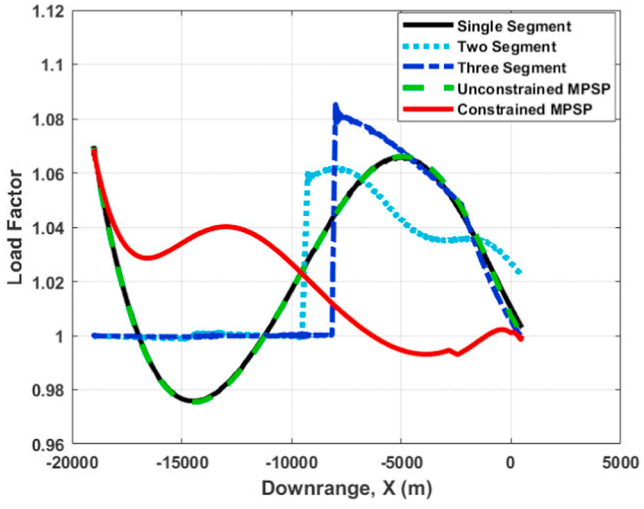

Fig. 5. Comparison of load factor for different guidance schemes

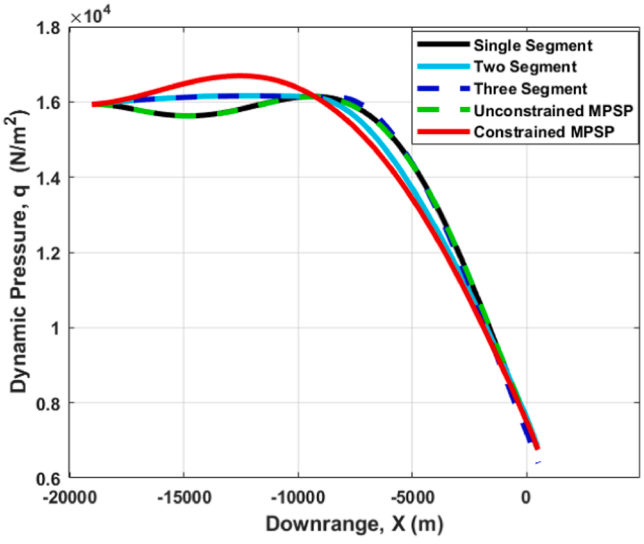

Fig. 6. Comparison of dynamic pressure for different guidance schemes

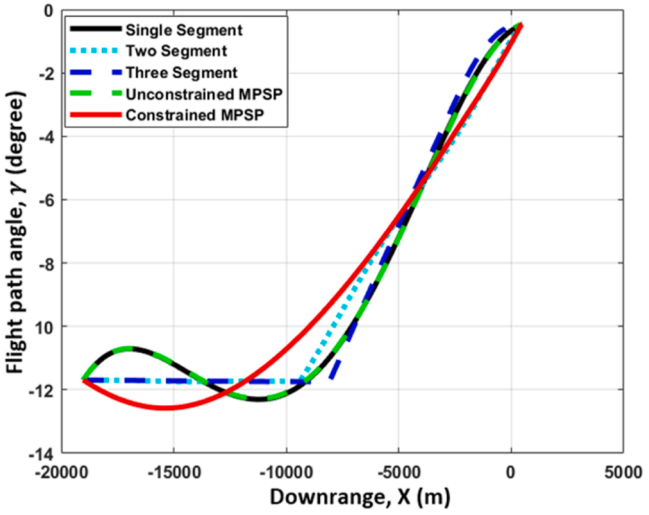

Fig. 7. Comparison of flight path angle for different guidance schemes

Table 4
Dispersion Ranges

Parameter	Dispersion range
Velocity, V	±5 %
Pitch angle, θ	±5 %
Altitude, h	±5 %
Coefficient of lift, C_L	±5 %
Coefficient of drag, C_D	±5 %
Mass, m	±3 %
Atmospheric density, ρ	±3 %

$$BB^i_{N-1} = \left[\frac{\partial Y^i_N}{\partial Z^i_N}\right] \tag{21}$$

Using (21), the matrix BB^i_k is computed for every step $k = (N-2),\ (N-3)\ldots 1$ using (22).

$$BB^i_k = BB^i_{k+1}\left[\frac{\partial F^i_{k+1}}{\partial Z^i_{k+1}}\right] \tag{22}$$

The matrix B^i_k can then be computed as in (23).

$$B^i_k = BB^i_k\left[\frac{\partial F^i_k}{\partial U^i_k}\right] \tag{23}$$

The system dynamics is propagated from the initial ALI to touchdown and the sensitivity matrices are computed at every step k. The sensitivity matrices B^i_k at each intermediate step k are calculated using (20) and the error in output states at the final step dY^i_N is obtained using (19). During this process, the control vector U^i_k is updated at every step $k = 1, 2\ldots N-1$ by minimizing a cost function J chosen as in (24).

$$J = \frac{1}{2}\sum_{k=1}^{N-1}\left(dU^i_k\right)^T R_k dU^i_k \tag{24}$$

dU^i_k is the deviation in control for each iteration of the MPSP algorithm. The cost function minimizes the deviation in control as indicated by (24). Similar to the assumption made in guidance design for re-entry phase [22], the assumption made in this paper is that the guess control history evaluated using a single segment-based guidance algorithm is accurate since it provides a feasible solution to drive the states close to the desired states at touchdown [21]. Hence, large fluctuations in the control input history is undesirable. By minimizing the deviations from the control input (for both angle of attack and pitch rate) at every step, the states are driven close to the desired values at touchdown. Therefore, the updated control history evaluated for every iteration U^{i+1}_k should remain close to the previous control history U^i_k. The error or deviation in control dU^i_k for each iteration is hence minimized using the selected cost function.

The updated control is obtained by subtracting the error given by dU^i_k from the previous control value. R_k is a positive definite matrix chosen judiciously by the control designer. R_k is the weighting matrix which distributes the control requirement to the control inputs starting from ALI to touchdown. It is initially chosen as unity and then re-tuned further to obtain a feasible solution by minimizing the cost function in the control update process. Using optimization theory, by incorporating the terminal constraint (19), the augmented cost function can be framed as (25) where λ^i is the costate variable [23].

$$J = \frac{1}{2}\sum_{k=1}^{N-1}\left(dU^i_k\right)^T R_k dU^i_k + \lambda^{iT}\left(dY^i_N - \sum_{k=1}^{N-1} B^i_k dU^i_k\right) \tag{25}$$

For the unconstrained MPSP problem, based on conditions of optimality, $\frac{\partial J}{\partial U_k} = 0$ and $\frac{\partial J}{\partial \lambda} = 0$. Further, doing the necessary algebraic manipulations, dU^i_k is obtained as in (26) [22,23]

$$dU^i_k = -{R^i_k}^{-1}{B^i_k}^T A^{-1}_\lambda dY^i_N \tag{26}$$

where

$$A_\lambda \triangleq \left[-\sum_{k=1}^{N-1} B^i_k R^{-1}_k {B^i_k}^T\right] \tag{27}$$

If U^{i+1}_k is the updated command input obtained on completing i^{th} iteration and k^{th} time step. The control history is updated at each step as in (28).

$$U^{i+1}_k = U^i_k - dU^i_k \tag{28}$$

To deal with the constrained problem, the input command vector U comprising of angle of attack α and pitch rate ω constrained for every step k and bounded by the constraints (10) and (11) is expressed as (29).

$$U_{kmin} \le U^{i+1}_k \le U_{kmax} \tag{29}$$

Substituting (28) in (29), (30) is obtained.

$$U^i_k - U_{kmax} \le dU^i_k \le U^i_k - U_{kmin} \tag{30}$$

Splitting (30) to two separate inequalities lead to (31).

$$\begin{bmatrix} I \\ -I \end{bmatrix} dU^i_k \le \begin{bmatrix} U^i_k - U_{kmin} \\ -\left(U^i_k - U_{kmax}\right) \end{bmatrix} \tag{31}$$

The optimization problem in the A & L phase hence reduces to minimization of the cost function (25) subject to the inequality constraint (31). The problem can be solved using standard quadratic programming methods like Sequential Quadratic Programming to arrive at a solution for dU^i_k.

The control history is thus updated at each step from ALI to touchdown as in (28). At the final step N, the error in output states given by $dY^i_N = Y^i_N - {Y^i_N}^d$ is calculated and compared with an allowed tolerance value. The iterations are continued until the error at touchdown converges within allowable limits.

Under perturbation in nominal states also, the control input needs to be iteratively updated by the MPSP algorithm to satisfy the touchdown conditions as well as control constraints. The solution obtained is sub-optimal due to the fact that the iterations of MPSP are terminated based on output convergence. The selection of the cost function with associated weighting factors is kept simple as in (24). The necessity of adding additional terms in the cost function in order to maintain continuity and smoothness in guidance commands (specifically required for multi-segment design) is eliminated. This advantage is achieved in the current design because the initial guess command history is selected

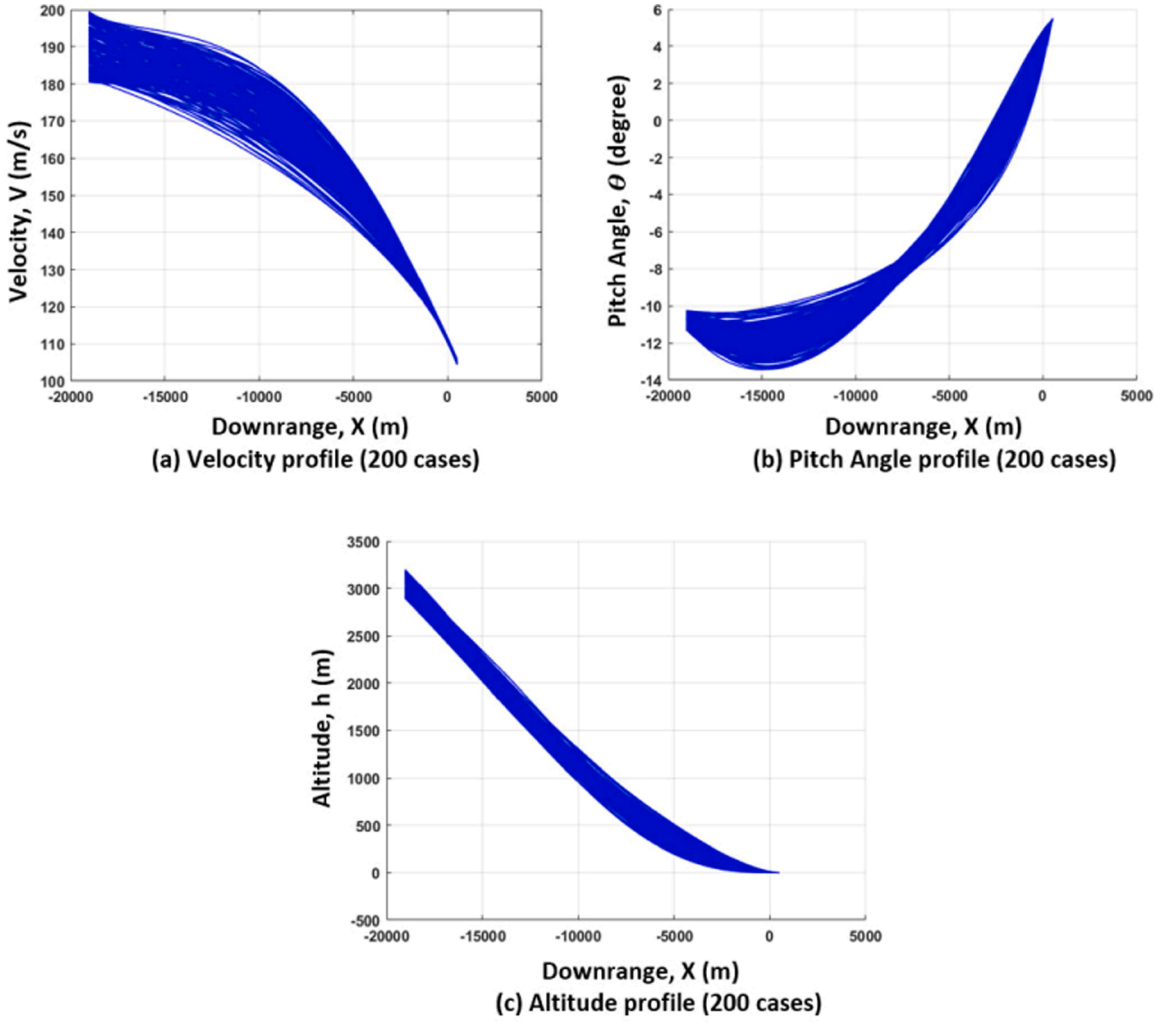

Fig. 8. Output profile under off-nominal conditions

such that the vehicle is guided through a single flight phase instead of transitioning through multiple trajectory segments. Moreover, the convergence of MPSP demands careful selection of a good initial guess control history. The requirement is met by adopting the control guess history based on a single segment design approach proposed in [21]. This approach aids in faster convergence of the MPSP based solution as well.

3. Determination of angle of attack and pitch rate guess control history

The angle of attack guess history is chosen based on a single segment approach as mentioned in the previous section. A quintic polynomial-based altitude model is used which is computationally faster and offers the advantages of a single flight phase avoiding the necessity of matching between multiple segments [21]. The relation between altitude h and downrange X is modelled as in (32). X_i=X_{ALI} is the downrange at A & L interface and $X - X_i$ is the ground track distance to be covered until touchdown on the runway [21].

$$h(X) = a_0 + a_1(X - X_i) + a_2(X - X_i)^2 + a_3(X - X_i)^3 + a_4(X - X_i)^4 + a_5(X - X_i)^5 \tag{32}$$

The six unknown coefficients of the quintic polynomial $a_0, a_1, a_2, a_3, a_4, a_5$ are determined from the boundary conditions on the vehicle states. The first derivative of altitude with respect to downrange is given by (33) which yields the reference flight path angle [21].

$$h'(X) = \tan\gamma = a_1 + 2a_2(X - X_i) + 3a_3(X - X_i)^2 + 4a_4(X - X_i)^3 + 5a_5(X - X_i)^4 \tag{33}$$

The boundary conditions on altitude, flight path angle and velocity at ALI (nominal values) as well as their desired values at the touchdown point are known. Therefore, it is possible to obtain six boundary conditions in order to compute the unknown coefficients $a_0, a_1, a_2, a_3, a_4, a_5$. The reference coefficient of lift during the entire phase is computed as in (34) [21].

$$C_L = \frac{mV^2\cos^3\gamma\, h''(X) + mg\cos\gamma}{qS} \tag{34}$$

where the second derivative of altitude is given by (35) [21].

$$h''(X) = 2a_2 + 6a_3(X - X_i) + 12a_4(X - X_i)^2 + 20a_5(X - X_i)^3 \tag{35}$$

The forward propagation algorithm is used to determine the reference trajectory parameters for the entire A & L phase. The angle of attack profile is a function of C_L and *Mach Number* as shown in (36) and is obtained under nominal conditions from [21] which drives the states close to the desired touchdown values.

$$\alpha = \alpha(C_L, Mach) \tag{36}$$

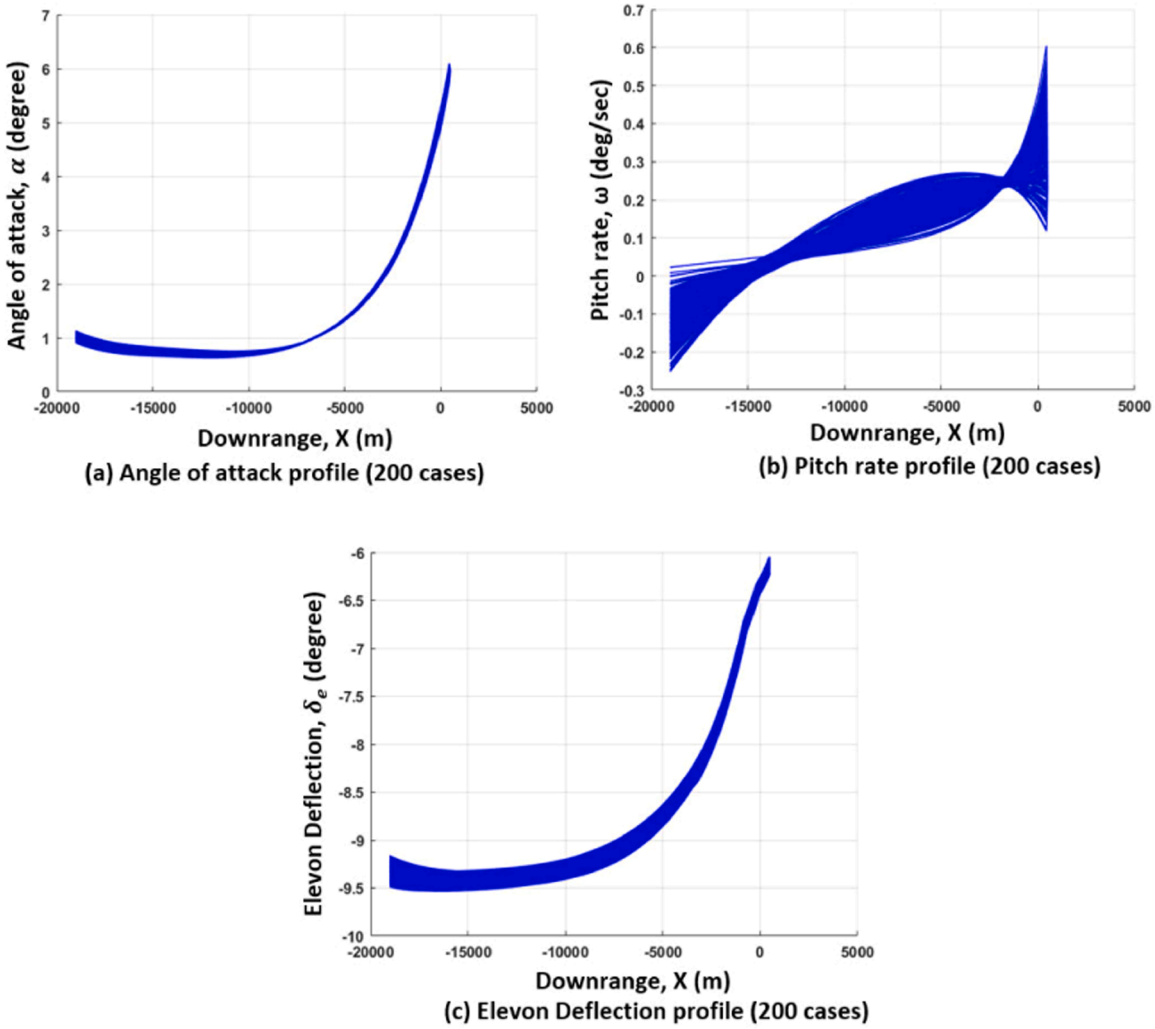

Fig. 9. Command profile under off-nominal conditions

Table 5
Touchdown results for simulated cases

Parameter	Mean value	Standard devation	Minimum value	Maximum value
Touchdown velocity, V_{TD} (m/s)	104.627	0.39	103.88	105.72
Touchdown pitch angle, θ_{TD} (deg)	5.558	0.081	5.3	5.69
Touchdown downrange, X_{TD}(m)	527.693	30.54	452.14	583.45
Touchdown sink rate, $\dot{h}_{TD}$ (m/s)	-0.743	0.151	-0.495	-1.21

This process is carried out only under the nominal initial conditions at ALI in order to compute the initial angle of attack guess history. The reference flight path angle from ALI to touchdown can be calculated from (33) under nominal initial conditions. This in turn facilitates the computation of pitch angle history for the entire phase since $\theta = \gamma + \alpha$. The initial pitch rate guess history can then be calculated as $\omega = \frac{d\theta}{dX} Vcos\gamma$ from (3).

Along with eliminating the requirement to ensure continuity in trajectory parameters, the additional advantage of MPSP formulation is that it allows for incorporating upper and lower bounds on the input commands in the design.

4. Computation of guidance command history

The control guess history is initially used by the MPSP algorithm to propagate the system dynamics from the nominal initial conditions at ALI to the touchdown point. The block diagram of the MPSP guidance algorithm implementation for A & L is as shown in Fig. 2. The angle of attack and pitch rate guess history obtained from single segment algorithm is initially used for state propagation for every step $k = 1, 2....N-1$. After each iteration, the error on output states is computed at touchdown. If the terminal error is within the tolerance limit, convergence is achieved and iterations are stopped. Otherwise, convergence criteria are not met and the iterations are continued to update the commands at every step k. The cost function is minimized at every step taking into account of the constraints on angle of attack and pitch rate. The guidance commands are updated at every step based on (37) and (38).

$$\omega_k^{i+1} = \omega_k^i - d\omega_k^i \tag{37}$$

$$\alpha_k^{i+1} = \alpha_k^i - d\alpha_k^i \tag{38}$$

The angle of attack and pitch rate command history for which the terminal and control constraints are satisfied is the converged solution $[\omega^* \quad \alpha^*]^T$ of the MPSP formulation.

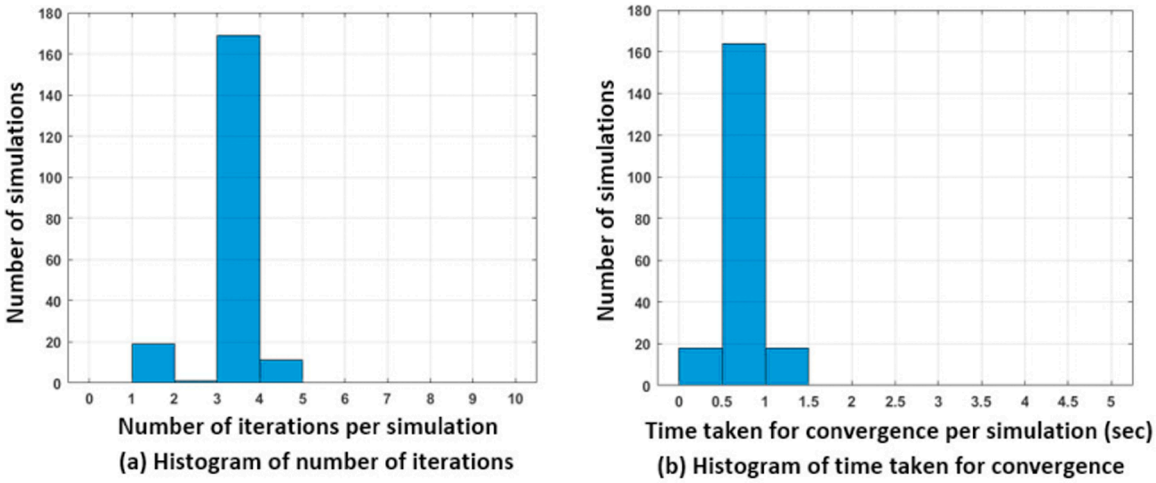

Fig. 10. Histogram of number of iterations and time taken for convergence

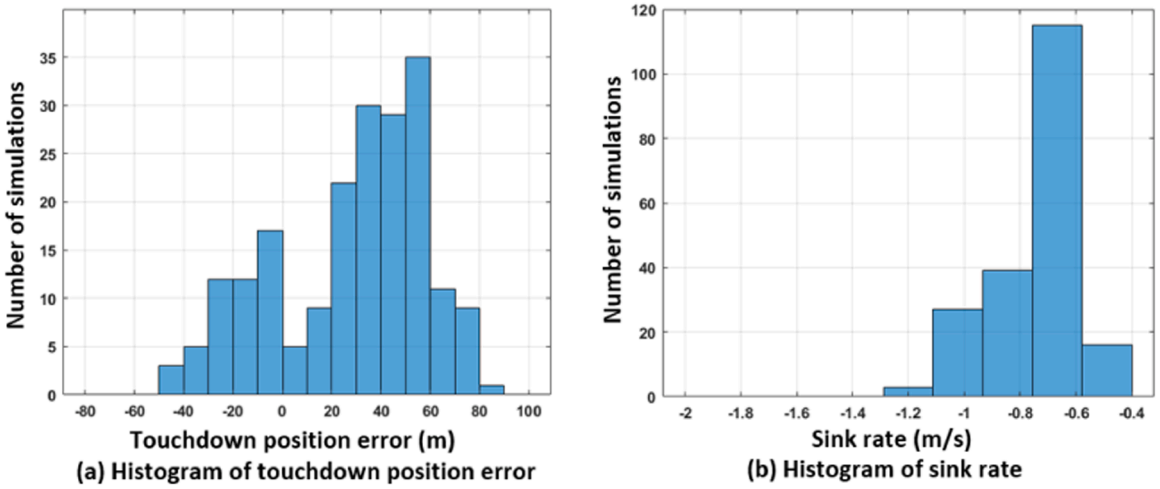

Fig. 11. Histogram of touchdown position error and sink rate

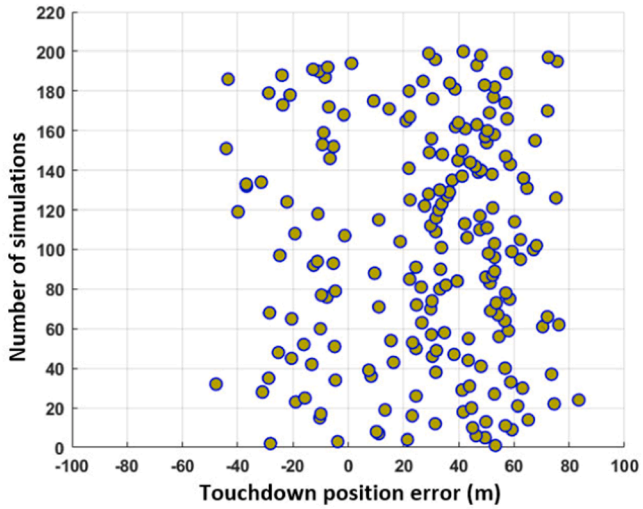

Fig. 12. Scatter plot of touchdown position error

4.1. Computation of elevon deflection angle

Dynamic inversion is used to accomplish the task of computing the elevon deflection required that will result in the vehicle attain the pitch rate history obtained from MPSP guidance. This can be achieved by enforcing first order error dynamics on the pitch rate as shown in (39).

$$\omega^{*'} - \omega' + k_\omega(\omega^* - \omega) = 0 \tag{39}$$

where k_ω is the pitch rate gain suitably chosen by the designer. The value of ω^* in (39) is obtained from the converged solution of the MPSP guidance algorithm. $\omega^{*'}$ for each guidance interval is taken as zero assuming that ω^* has small variations even though its value is updated at every grid point. Hence,

$$\omega' = k_\omega(\omega^* - \omega) \tag{40}$$

The longitudinal pitch rate dynamics ω' in (4) can be written as shown in (41).

$$\omega' = \frac{0.5\rho V S\overline{c}\left(C_{M0} + C_{M\alpha}\alpha + C_{M\delta_e}\delta_e + \frac{R(C_L\cos\alpha + C_D\sin\alpha)}{\overline{c}}\right)}{I_{yy}\cos\gamma} \tag{41}$$

Substituting the desired dynamics ω' from (40) to the inherent system dynamics (41) and performing the necessary algebra, the elevon

deflection obtained using dynamic inversion is as shown in (42).

$$\delta_e = C_{M\delta_e}^{-1}\left(\frac{k_\omega(\omega^* - \omega)I_{yy}\cos\gamma}{0.5\rho VS\bar{c}} - \left[\frac{R(C_L\cos\alpha + C_D\sin\alpha)}{\bar{c}}\right] - C_{M0} - C_{M\alpha}\alpha\right) \tag{42}$$

Eq. (42) represents the history of elevon deflection required to achieve the desired pitch rate history predicted by the MPSP algorithm.

5. Results and discussion

Simulations are performed under both nominal and off-nominal conditions. Comparison is carried out between unconstrained and constrained MPSP for nominal conditions and the results clearly indicate the superior performance of the constrained scheme. The effectiveness of the constrained scheme is especially evident in curtailing the transient variation in pitch angle and flight path angle. The results obtained from simulations of multiple variations under off-nominal conditions also reiterates the suitability of the proposed scheme for high precision landing in short runways.

5.1. Nominal conditions

The nominal initial conditions at ALI as well as desired touchdown conditions are specified in Table 1 and Table 2 respectively. The convergence criteria for the output error in terminating the MPSP iterations are shown in Table 3.

Comparison is carried out between unconstrained and constrained MPSP and the profile of different states obtained for nominal initial conditions are shown in Fig. 3. The profile for velocity and altitude shows minimal variations between the unconstrained and constrained cases. The pitch angle profile obtained for constrained MPSP shows a smoother variation compared to that of the unconstrained case. The profile for angle of attack, pitch rate and elevon deflection are shown in Fig. 4. Variation between the two cases is evident especially in the pitch rate command. For constrained MPSP, it is observed that the transient variations in the pitch rate command occurring for the unconstrained case is modified to arrive at a gradually increasing profile.

5.2. Comparison of different guidance strategies

Different guidance strategies are compared to evaluate the relative advantages of the proposed scheme. The different guidance strategies used for comparison with the proposed scheme make use of PID control for generating closed loop guidance commands. The guidance strategies used are (i)a three-segment guidance algorithm (steep glideslope, circular pull-up, flare) detailed in [5], reimplemented on the X34 vehicle model (ii) a two-segment guidance scheme (steep glideslope followed by quadratic flare maneuver) explained in [6] with PID control as detailed in [5] (iii) a single segment scheme designed in [21]. The advantages offered by constrained MPSP is evaluated by comparing the load factor profile, dynamic pressure profile and flight path angle profile for all the above-mentioned schemes.

The load factor (the ratio of the lift force to the component of weight normal to the flight path) is plotted for the different schemes and the result is presented in Fig. 5. During initial glideslope phase, the load factor remains constant for two segment as well as three segment schemes, thereafter there is a sharp upward transition observed in load factor due to the transition happening to the next flight phase. This sharp transition is absent in the case of both constrained and unconstrained MPSP, since MPSP strategy relies on a single segment-based flight phase for the entire A & L. The load factor for unconstrained MPSP is mostly observed to be coinciding to that of the single segment guidance strategy. However, compared to both the unconstrained MPSP and single segment schemes, the constrained MPSP scheme offers lesser load factor which keeps on decreasing from the initial value at ALI to touchdown. The range of variation of load factor from ALI to touchdown do not show a large difference between the schemes. But, unlike other schemes, it is observed that the load factor for constrained MPSP does not exhibit the tendency to transition between the lowest to a highest peak value and shows a gradual variation. The change in load factor for constrained MPSP is observed to be much lesser compared to that of other schemes.

Fig. 6 represents the comparison of dynamic pressure for the different schemes. There is an initial increase observed in the dynamic pressure for constrained MPSP due to a relatively gradual decrease in velocity. However, as the vehicle starts descending further, the dynamic pressure for constrained MPSP is observed to be the least for major part of the downrange until touchdown.

Flight path angle for all the strategies is compared in Fig. 7. It is observed that the flight path angle remains constant during the initial glideslope phase for three-segment as well as two-segment schemes. But owing to a single flight phase for the single segment scheme, flight path angle exhibits an initial wavy transition which is undesirable and has been cited as a limitation of the single segment algorithm [21]. The same limitation occurs in unconstrained MPSP as well. However, a major advantage offered by the constrained MPSP is that the initial vibratory nature of the flight path angle profile is smoothened out and the profile exhibits a gradual variation.

The analysis indicates that by adopting the constrained MPSP strategy, the advantages offered by the single flight phase are retained and at the same time, the flight path angle profile is smoothened out by constraining the input commands within bounds. This is achieved without phenomenal increase in load factor or dynamic pressure thereby preserving the structural safety of the vehicle.

5.3. Off-nominal conditions

The performance of the algorithm is evaluated with random dispersion in initial states, aerodynamic coefficients C_L and C_D, mass and atmospheric density. In the presence of these random variations, 200 simulations are carried out to analyze the effect on touchdown conditions. The focus here is to evaluate the effectiveness of the algorithm for precise landing, under unfavorable conditions. Dispersion ranges for perturbation analysis are indicated in Table 4.

As represented in Table 4, the initial velocity, pitch angle and altitude have uniform distributions with mean value equal to the nominal states at ALI and the limits applied as ±5% from the nominal value. The dispersion range of ±5% is applied for aerodynamic coefficients throughout the sample points considered from ALI to touchdown. The variation in vehicle mass is taken as ±3% and dispersion in atmospheric density is considered as ±3% throughout the A & L phase.

The profile of the output obtained by running 200 cases with all the considered variations are shown in Fig. 8. In the presence of random simultaneous state and parameter variations indicated as in Table 4, all the output states are found to converge at touchdown. The profile of angle of attack, pitch rate as well as the elevon deflection obtained are shown in Fig. 9 for all the simulated cases. The statistics of the touchdown states with the mean and standard deviation along with minimum and maximum values obtained from all the 200 cases is shown in Table 5.

The results in Table 5. can be analyzed with respect to practical issues that happen on unpowered landing like tire blowout, tail scraping, colliding with runway and overrunning the runway length. Minimal variations occur in the touchdown velocity ranging between 103.88 m/s and 105.72 m/s. The touchdown velocities for all cases remain very close to the desired value of 105 m/s, leaving least possibility for tire blow out. The pitch angle at touchdown and the final sink rate are indicative of the fact that tail scraping is avoided with the vertical velocity within safe limits to avoid hard impact on landing. The runway length for landing facility of unpowered RLVs are usually of the order of 4 to 5 km. Hence, a maximum position error of 83.45 m beyond the desired touchdown downrange position of 500 m, despite all the

unfavorable conditions, is considered to be offering a high precision upon landing.

Simulations are performed in MATLAB environment with an i7-10750H processor and 16 GB RAM. A histogram of the number of iterations taken per simulation as well as time taken for convergence for each simulation is shown in Fig. 10 (a) and (b). Even under off-nominal conditions, the time taken for convergence is within 1.5 sec for each simulation. Histogram of the touchdown position error as well as sink rate are shown in Fig. 11 (a) and (b). The sink rate for majority of the cases is between -0.8 m/s and -0.6 m/s and is safe for touchdown for all the cases.

The scatter plot of touchdown position error for all the 200 simulations is shown in Fig. 12. indicating that at touchdown, the position error from the desired point is within -48 m and + 84 m for all the simulations. It demonstrates that the MPSP technique is capable of delivering RLV to the desired touch down point with high precision under off-nominal conditions. The simulation results hence indicate a strong feasibility of implementing constrained MPSP for landing of RLVs especially on runways of shorter lengths.

6. Conclusion

A constrained Model Predictive Static Programming based guidance algorithm is proposed in this paper for the unpowered A & L phase of a reusable launch vehicle. The design is accomplished with the advantage of a single segment approach eliminating the necessity of ensuring continuity between multiple segments, followed in traditional design approaches. This leads to a simple cost function without the need for additional terms to ensure continuity in commands. Moreover, the solution is obtained by imposing constraints on the control inputs throughout the entire phase which limits the control surface deflection within allowable bounds. A guess control history is initially computed based on single segment approach under nominal conditions and the deviation in control effort is minimized throughout the entire phase satisfying both control constraints as well as terminal constraints at touchdown. The implementation of constrained MPSP brings in the inherent advantages like static costate vector and recursive computation of sensitivity matrices for reducing the computation time to arrive at the converged solution. Closed loop guidance is implemented and the results are compared between unconstrained and constrained MPSP methods. The comparison of load factor, dynamic pressure and flight path angle for three segment, two segment and single segment guidance strategies with both unconstrained and constrained MPSP brings out the relative advantages of the proposed scheme. The performance is evaluated by considering simultaneous variations in parameters under off-nominal conditions. Numerical results indicate that the algorithm is effective for precise landing with minimal error on a designated site under unfavorable conditions and can be applied for landing on runways of shorter lengths.

As a future scope, Monte-Carlo simulations may be carried out to evaluate the accuracy obtained in the touchdown states for the actual engineering application. Moreover, aerodynamic coefficient errors for pitching moment can be considered in simulations to further evaluate the results obtained at touchdown. Such errors may be significant due to the uncertainties in the location of center of pressure of the vehicle. More investigations are needed with an adequate wheel/ground interaction model to understand the effect of the shock at touchdown on the length of the track and comes under the future scope of the work.

Declaration of Competing Interest

The authors declare that they have no known competing financial interests or personal relationships that could have appeared to influence the work reported in this paper.

Data Availability

No data was used for the research described in the article.

References

[1] G M Tsikalas, Space shuttle autoland design, AIAA Paper 82-1604-CP (1982).
[2] G. H. Barton, S. G. Tragesser, Autolanding Trajectory Design for the X-34, AIAA Paper 99- 4161 (1999).
[3] A. Girerd, Onboard Trajectory Generation for Unpowered Landing of Autonomous Reusable Launch Vehicles, Massachusetts Institute of Technology/Charles Stark Draper Laboratory T-1390, 1997. M.S. Thesis.
[4] C.A. Kluever, D. Neal, Approach and landing range guidance for an unpowered reusable launch vehicle, J. Guid. Control Dyn. 38 (2015) 2057–2066.
[5] C.A. Kluever, Unpowered approach and landing guidance using trajectory planning, J. Guid. Control Dyn. 27 (2004) 967–974.
[6] S.H. Aysha, G.R. Bindu, A novel flare maneuver guidance for approach and landing phase of a reusable launch vehicle, in: 2019 Advances in Science and Engineering Technology International Conferences (ASET), Dubai, 2019.
[7] S.H. Aysha, G.R. Bindu, Gain scheduled finite horizon LQR for approach and landing phase of a reusable launch vehicle, J. Inst. Eng. India Ser. C (2022).
[8] C.T. Chomel, Design of a Robust Integrated Guidance and Control Algorithm for the Landing of a Autonomous Reusable Launch Vehicle, Dept. of Aeronautics and Astronautics, Massachusetts Inst. of Technology, Cambridge, 1998. M.S. Thesis.
[9] X Liu, F. Zhang, Z. Li, Y. Zhao, Approach and landing guidance design for reusable launch vehicle using multiple sliding surfaces technique, Chinese J. Aeronaut. 30 (2017) 1582–1591.
[10] Y. Zhao, Y Sheng, X Liu, Z Li, Analytic approach and landing guidance through a novel time varying sliding mode control method, J. Aerosp. Eng. 29 (2016).
[11] D.M.K.K Venkateswara Rao, T.H Go, Automatic landing system design using sliding mode control, Aerosp. Sci. Technol. 32 (2014).
[12] A. Heydari, S.N. Balakrishnan, Optimal online path planning for approach and landing guidance, in: AIAA Atmospheric Flight Mechanics Conference 2011-6641, 2011.
[13] A. Heydari, S.N. Balakrishnan, Path planning using a novel finite horizon suboptimal controller, J. Guid. Control Dyn. 36 (2013) 1210–1214.
[14] X Yan, L He, Unpowered approach and landing trajectory planning using second-order cone programming, Aerosp. Sci. Technol. 101 (2020).
[15] M Li, J Hu, An approach and landing guidance design for reusable launch vehicle based on adaptive predictor-corrector technique, Aerosp. Sci. Technol. 75 (2018).
[16] M Pagone, C Novara, P Martella, C Nocerino, GNC robustness stability verification for an autonomous lander, Aerosp. Sci. Technol. 100 (2020).
[17] M Lungu, Backstepping and dynamic inversion combined controller for auto-landing of fixed wing UAVs, Aerosp. Sci. Technol. 96 (2020).
[18] M Lungu, Auto-landing of UAVs with variable center of mass using the backstepping and dynamic inversion control, Aerosp. Sci. Technol. 103 (2020).
[19] M Lungu, Backstepping and dynamic inversion control techniques for automatic landing of fixed wing unmanned aerial vehicles, Aerosp. Sci. Technol. 120 (2022).
[20] Y Lim, A Gardi, R Sabatini, K Ranasinghe, N Ezer, K Rodgers, D Salluce, Optimal energy-based 4D guidance and control for terminal descent operations, Aerosp. Sci. Technol. 95 (2019).
[21] S.H. Aysha, G.R. Bindu, Single segment approach and landing guidance and control for an unpowered reusable launch vehicle, Aerosp. Sci. Technol. 115 (2021).
[22] O. Halbe, R.G. Raja, R. Padhi, Robust reentry guidance of a reusable launch vehicle using model predictive static programming, J. Guid. Control Dyn. 37 (2013) 134–148.
[23] C. Chawla, P. Sarmah, R. Padhi, Suboptimal reentry guidance of a reusable launch vehicle using pitch plane maneuver, Aerosp. Sci. Technol. 14 (2011) 269–282.
[24] G. Brauckmann, X-34 vehicle aerodynamic characteristics, J. Spacecr. Rockets. 36 (1999) 229–239.
[25] B.N. Pamadi, G.J. Brauckmann, M.J. Ruth, H.D. Fuhrmann, Aerodynamic characteristics, database development and flight simulation of the X-34 vehicle, J. Spacecr. Rockets. 38 (2001) 334–344.
[26] R. Padhi, M. Kothari, Model predictive static programming: a computationally efficient technique for suboptimal control design, Int. J. Innov. Comput. Inf. Control. 5 (2009) 377–386.
[27] A. Maity, R. Padhi, A suboptimal guidance design using continuous-time MPSP with input inequality constraint in a hypersonic mission, in: IFAC Proceedings Volumes 43, 2010.
[28] A.K. Tripathi, R. Padhi, Autonomous landing of UAVs using T-MPSP and Dynamic Inversion Autopilot, IFAC Papers Online 49 (2016) 18–23.
[29] P. Kumar, B.B. Anoohya, R. Padhi, M. Kothari, Model predictive static programming for optimal command tracking: a fast model predictive control paradigm, J. Dyn. Sys. Meas. Control. 141 (2019).
[30] Farhad Tavakoli, Alireza Basohbat Novinzadeh, Designing a closed-loop guidance system to increase the accuracy of satellite-carrier boosters' landing point, Aerosp. Sci. Technol. 76 (2018).
[31] Promod Pashupathy, Arnab Maity, Haichao Hong, Florian Holzapfel, Unspecified final-time nonlinear suboptimal guidance of aerobatic aircraft in air race, Aerosp. Sci. Technol. 116 (2021).
[32] Cong Zhou, Xiaodong Yan, Shuo Tang, Generalized quasi-spectral model predictive static programming method using Gaussian quadrature collocation, Aerosp. Sci. Technol. 106 (2020).